AIAA JOURNAL
Vol. 38, No. 7, July 2000

Unsteady Swirling Flows in Annular Cascades, Part 2: Aerodynamic Blade Response

Vladimir V. Golubev* and Hafiz M. Atassi†
University of Notre Dame, Notre Dame, Indiana 46556

A model is developed for the interaction of unsteady incident disturbance in a swirling mean motion with an annular cascade of unloaded blades. The incident disturbances are modeled by using a combined eigenmode analysis with initial-value problem solutions as described elsewhere (Golubev, V. V., and Atassi, H. M., "Unsteady Swirling Flows in Annular Cascades, Part 1: Evolution of Incident Disturbances," *AIAA Journal*, Vol. 38, No. 7, 2000, pp. 1142–1149). The scattered field is calculated in response to the blade upwash and accounts for the effects of the centrifugal and Coriolis forces induced by the mean swirl. Benchmark results are presented for the unsteady blade pressure in the rotor-wake/stator interaction problem. These results are compared with the strip theory and show strong dependence on the swirl-induced changes in the radial distribution and axial evolution of the incident vortical disturbances.

Introduction

THE modeling of the unsteady aerodynamics of an annular cascade of airfoils was first developed in the two-dimensional approximation wherein the annular cascade is unrolled into a linear cascade of infinite blades. In this approximation the centrifugal and Coriolis forces resulting from the fluid circumferential motion or swirl are assumed to be negligible. The linear cascade can be regarded as a model for the annular cascade in the limit, where the hub and tip radii r_h and r_t are very large but $(r_t - r_h)/r_h$ is small and the circumferential velocity U_S is finite. Using this model to study the interaction of a cascade with unsteady incident disturbances, it is possible to assume that the upstream mean flow is uniform. Moreover, for a flat-plate unloaded linear cascade the unsteady velocity field can be split into a known incident vortical disturbance convected by the uniform mean flow and a scattered potential disturbance produced in response to the incident vortical disturbance upwash along the blade surface.[1] The problem is then formulated in terms of a singular integral equation.[2,3] Numerical solutions are obtained for the unsteady blade pressure[4,5] and the upstream and downstream acoustic radiation.[6,7] The corresponding results for an annular cascade are then obtained from the two-dimensional formulation using the strip theory approximation.

For a loaded linear cascade in an inviscid potential mean flow, it is always possible to split the unsteady velocity into vortical and potential disturbances. However, the vortical disturbances are no longer simply convected but undergo significant distortions as they are carried downstream by the spatially varying mean flow.[1,8,9] Moreover, the potential disturbance field is governed by nonconstant coefficients partial differential equations. A computationally efficient approach for mean potential flows was developed in Ref. 10, which accounts for the mean flow distortion of the vortical disturbances but neglects higher-order nonlinear and viscous effects. Based on this approach, numerical solutions have been obtained for the problem of unsteady disturbances interacting with loaded two-dimensional airfoils[11] and cascades.[12,13]

More recently, computational models were developed that consider the three-dimensional geometry of the annular cascade. Namba[14] developed a singularity method that accounts for the annular duct geometry and spanwise nonuniformity of the incident disturbances. However, singularity methods cannot account for the effects of nonuniform mean flow. A linearized Euler analysis was also developed by Montgomery and Verdon.[15] This analysis, however, assumes the gust to be simply convected by the mean flow at the inflow/outfow boundaries, and thus may not account for the important changes in amplitude and phase of the incoming disturbances caused by the mean swirl.

In Part 1, we have analyzed the evolution of unsteady incident disturbances in a swirling mean flow in an annular duct. The centrifugal and Coriolis forces associated with the mean motion couple the pressure and vortical disturbance modes. As a result, it is no longer possible to split, as for a uniform flow, the disturbances into separate pressure (acoustic) and convected vortical modes. However, an eigenmode analysis[17,18] revealed that the eigenmodes can be segregated into pressure-dominated and vorticity-dominated modes. The latter have eigenvalues that accumulate with increasing density near a critical layer. The analysis also indicated that these eigenmodes do not form a complete set. These results prompted us to describe the upstream gust in terms of the eigenmodes and of solutions to an intial-value problem. The initial-value solutions represent transient vorticity–acoustic waves coupled by the mean flow vorticity. These waves evolve toward stable steady-state oscillations, decay, or amplify depending on the radial variation of the mean swirl, i.e., the machine design.

The objective of the present paper is to analyze the interaction of an unsteady upstream disturbance in a swirling mean motion with a three-dimensional cascade of unloaded blades. A model is developed wherein the scattered field is calculated in response to the blade upwash resulting from an incident gust evolving in a mean swirling flow. Our goal is to present benchmark results and to quantify the effects of the mean swirl on the unsteady pressure response of the blades. In what follows, we present the formulation of our model in terms of a coupled system of equations and define the corresponding boundary-value problem and its inflow/outflow conditions. The analysis is then applied to the rotor/stator interaction problem, and the results for the unsteady blade pressure are presented and compared with those of strip theory calculations.

Governing Equations

We assume, as in Ref. 16, that the unsteady part of the flow quantities are small disturbances about the corresponding mean values. Thus, the total velocity can be written as

$$\boldsymbol{V}(\boldsymbol{x}) = \boldsymbol{U}(\boldsymbol{x}) + \boldsymbol{u}(\boldsymbol{x}, t) \tag{1}$$

where $|\boldsymbol{u}| \ll |\boldsymbol{U}|$ and similar expressions for the pressure and density. We use cylindrical coordinates (see Ref. 16, Fig. 1), where the x axis is aligned with the machine axis and r and θ represent the radial distance and the circumferential angle, respectively. The mean flow

Presented as Paper 97-1634 at the 3rd Joint CEAS/AIAA Aeroacoustics Conference, Atlanta, GA, 12–14 May 1997; received 13 September 1999; revision received 2 November 1999; accepted for publication 2 November 1999.

*Research Associate, Department of Aerospace and Mechanical Engineering. Member AIAA.
†Viola D. Hank Professor, Department of Aerospace and Mechanical Engineering. Fellow AIAA.

velocity $\boldsymbol{U}(\boldsymbol{x})$ is assumed to have axial and swirl components that depend only on the radial distance r

$$\boldsymbol{U}(\boldsymbol{x}) = U_x(r)\hat{e}_x + U_s(r)\hat{e}_\theta \tag{2}$$

where

$$U_s = \Omega r + \Gamma/r \tag{3}$$

$\hat{e}_x$ and $\hat{e}_\theta$ are the unit vectors in the axial and circumferential directions, respectively, and Γ and Ω are constants describing a free vortex and a rigid body mean flow rotations, respectively. For simplicity, we assume as in Ref. 16 that the axial velocity is coupled to the swirl velocity by the condition of uniform stagnation enthalpy across the annulus. This determines $U_x(r)$ in terms of $U_s(r)$ and U_0, the latter being the axial velocity specified at the mean radius of the annulus r_m [Eqs. (4) and (8) of Ref. 16].

We further decompose the unsteady velocity into vortical and potential components

$$\boldsymbol{u} = \boldsymbol{u}^{(R)} + \nabla\phi \tag{4}$$

and assume that the unsteady pressure is determined solely in terms of the potential function

$$p' = -\rho_0 \frac{\mathrm{D}_0\phi}{\mathrm{D}t} \tag{5}$$

This has the advantage of associating the vorticity with $\boldsymbol{u}^{(R)}$ and the unsteady pressure with ϕ. Substituting Eqs. (4) and (5) into the unsteady linearized Euler equations, we obtain the following coupled equations for the vortical velocity $\boldsymbol{u}^{(R)}$ and potential ϕ:

$$\mathcal{L}_c\boldsymbol{u}^{(R)} = -\zeta_0 \times \nabla\phi \tag{6}$$

$$\mathcal{L}_w\phi = (1/\rho_0)\nabla\cdot\left[\rho_0\mathbf{u}^{(R)}\right] \tag{7}$$

where $\mathcal{L}_c$ and $\mathcal{L}_w$ are, respectively, the operators of convection and wave propagation:

$$\mathcal{L}_c\boldsymbol{u}^{(R)} \equiv \frac{\mathrm{D}_0\boldsymbol{u}^{(R)}}{\mathrm{D}t} + \left[\boldsymbol{u}^{(R)}\cdot\nabla\right]\boldsymbol{U} \tag{8}$$

and

$$\mathcal{L}_w\phi \equiv \frac{\mathrm{D}_0}{\mathrm{D}t}\frac{1}{c_0^2}\frac{\mathrm{D}_0}{\mathrm{D}t}\phi - \frac{1}{\rho_0}\nabla\cdot(\rho_0\nabla)\phi \tag{9}$$

$\mathrm{D}_0/\mathrm{D}t = \partial/\partial t + \boldsymbol{U}\cdot\nabla$ is the convective derivative, ζ_0 is the mean flow vorticity, and ρ_0 and c_0 are the mean flow density and speed of sound, respectively. Equations (6) and (7) clearly show that in a swirling mean flow the unsteady pressure and vorticity are coupled, i.e., the unsteady pressure will produce an associated vortical field, and the unsteady vorticity will create an associated pressure field.

The eigenmode analysis[18] of Eqs. (6) and (7) shows that the eigenvalues are segregated into nearly sonic and nearly convected zones. This suggests that we consider

$$\boldsymbol{u}^{(R)} = \boldsymbol{u}^{(R)}_{(s)} + \boldsymbol{u}^{(R)}_{(c)}, \qquad \phi = \phi_{(s)} + \phi_{(c)} \tag{10}$$

where the subscript s denotes solutions propagating at nearly sonic velocities in the mean flow frame of reference and c, those nearly convected. Moreover, the eigenmode analysis shows that the unsteady pressure is dominated by the s modes, whereas the unsteady vorticity field is dominated by the c modes.

In the present analysis of unsteady fluid-structure interaction problem, upstream imposed incident disturbances can be represented in terms of s modes and/or c modes. For s-modes incident disturbances an eigenmode analysis of the unsteady swirling motion is used to describe the incident perturbations. For c-modes incident disturbances the initial-value analysis developed in Ref. 16 is used to describe the evolution of the vortical disturbances, which generalizes the concept of a gust to vortical swirling flows.

The interaction of upstream imposed incident disturbances with a cascade of unloaded blades produces a scattered velocity field, i.e., the cascade response, by means of satisfying the impermeability condition along the blade surface. The scattered field creates unsteady pressure loading along the blade surface and radiates sound in the upstream and downstream far fields. The analysis developed in Ref. 16 gives the expression for $\boldsymbol{u}^{(R)}_{(c)}$ and $\phi_{(c)}$. The scattered field is then determined by solving the coupled equations (6) and (7) for $\boldsymbol{u}^{(R)}_{(s)}$ and $\phi_{(s)}$ subject to the impermeability condition along the blade surface and nonreflecting radiation conditions at the inlet and outlet.

Application to Turbomachinery

We now focus our attention on the problem of turbomachine two-row interation. We consider a nonuniform flow with a mean swirl downstream of a rotor (stator) with B blades and angular velocity Ω_R and examine its interaction with a downstream stator (rotor) with N_b blades. In both cases the large-scale structure associated with the wake-induced velocity $\boldsymbol{u}_{(i)}$ is viewed in the upstream row frame of reference as stationary and periodic in the circumferential direction. Hence,

$$\boldsymbol{u}_{(i)} = \sum_m \boldsymbol{B}_m(x, r)\exp(im\theta) \tag{11}$$

where $\boldsymbol{B}_m(x, r)$ is the amplitude vector of the m harmonic, which is a multiple integer of the number of blades in the upstream row, and θ is the circumferential angle in the upstream row frame of reference. In the downstream row frame of reference, $\boldsymbol{u}_{(i)}$ appears as a time-dependent wave of the form

$$\boldsymbol{u}_{(i)}(x, r, \theta; t) = \sum_m \boldsymbol{B}_m(x, r)\exp[i(m\theta' - \omega t)] \tag{12}$$

where $\omega = m\Omega_R$. $\boldsymbol{B}_m(x, r)$ is determined numerically in terms of $\boldsymbol{B}_m(x_0, r)$ using an eigenmode and/or an initial-value analysis. θ' is the circumferential angle in the downstream frame of reference. In particular, the evolution of the wake-induced vortical perturbation is obtained from the initial-value analysis presented in Part 1 of this paper.[16] Without loss of generality, we consider a single (ω, m) Fourier component of Eq. (12):

$$\boldsymbol{B}_m(x, r) = \boldsymbol{A}_m(x, r) + \nabla\phi_{(c)m}(x, r) \tag{13}$$

which is expressed in terms of the vortical velocity amplitude $\boldsymbol{A}_m(x_0, r)$ and its associated potential part $\nabla\phi_{(c)m}(x, r)$, whose expressions are given in Ref. 16.

The blade upwash caused by Eq. (12) will produce a scattered field whose potential part is denoted by the potential function $\phi_{(s)}$ and whose vortical part is denoted $\boldsymbol{u}^{(R)}_{(s)}$. Because of the linearity of the problem, the unsteady loading and sound radiated from the blades will be at the same frequency ω. Thus, we can factor out the time dependence for the scattered field by introducing

$$\phi_{(s)}(x, r, \theta; t) = \hat{\phi}_{(s)}(x, r, \theta)e^{-i\omega t} \tag{14}$$

$$\boldsymbol{u}^{(R)}_{(s)}(x, r, \theta; t) = \hat{\boldsymbol{u}}^{(R)}_{(s)}(x, r, \theta)e^{-i\omega t} \tag{15}$$

where $\phi_{(s)}$ and $\boldsymbol{u}^{(R)}_{(s)}$ must satisfy Eqs. (6) and (7) with the upwash conditions along the blade's surface and nonreflecting conditions at the inlet and outlet of the computational domain.

For typical fan engines B and N_b are usually large numbers of about 20 and 40, respectively. If, for example, the rotor is upstream and is rotating with an angular velocity Ω_R, then upstream flow nonuniformities will be seen in the stator frame of reference as propagating waves with a fundamental frequency $\omega = B\Omega_R$. The nondimensional frequency $\tilde{\omega} = \omega r_m/U_0 = \mathcal{O}(B)$ is therefore large. This suggests nondimensionalization of lengths with respect to r_m (denoted with the superscript $*$) when variations of mean flow quantities such as the mean flow vorticity $\zeta_0^* = \zeta_0 r_m/U_0$ are considered and with respect to blade spacing $2\pi r_m/N_b$ (denoted with the superscript $'$) for unsteady flow spatial variations. Time will be nondimensionalized with respect to $1/\omega$ and the mean velocities, with respect to U_0.

Equation (6) can then be rewritten as

$$\left(\frac{\partial}{\partial t^*} + \frac{\alpha_s N_b}{2\pi B}\boldsymbol{U}^*\cdot\nabla'\right)\boldsymbol{u}^{(R)} + \frac{\alpha_s}{B}\boldsymbol{u}^{(R)}\cdot\nabla^*\boldsymbol{U}^* = \frac{\alpha_s}{B}\zeta_0^*\times\nabla'\phi \tag{16}$$

where $\alpha_s = U_0/r_m\Omega_R = \mathcal{O}(1)$.

Because we are considering a scattered particular solution of Eq. (6), Eq. (16) implies that $\boldsymbol{u}^{(R)}_s = \mathcal{O}(1/B)$ and may be neglected

to first order. This result concurs with our eigenvalue analysis, which shows that the right-hand side $\zeta_0 \times \nabla\phi_{(s)}$ scales with $\Omega\nabla\phi_{(s)}$, whereas the left-hand side $\mathcal{L}_c \boldsymbol{u}_{(s)}^{(R)}$ scales with $\Lambda_{mn}\boldsymbol{u}_{(s)}^{(R)}$, where $\Lambda_{mn} = -\omega + k_{mn}U_x + mU_s/r$ is an eigenvalue of the convected operator $\mathrm{D}_0/\mathrm{D}t$. The latter involves modal axial, circumferential, and radial wave numbers k_{mn}, m, and n, respectively. As shown for the test cases below, $|\Lambda_{mn}| \gg \Omega$ for the nearly sonic modes. As a result, $|\boldsymbol{u}_{(s)}^{(R)}| \ll |\nabla\phi_{(s)}|$.

This suggests the following asymptotic expansion:

$$\phi_{(s)} = \phi_{(s)}^{(0)} + (1/B)\phi_{(s)}^{(1)} + \cdots \tag{17}$$

$$\boldsymbol{u}_{(s)}^{(R)} = (1/B)\boldsymbol{u}_{(s)}^{(R)(1)} + \cdots \tag{18}$$

Substituting Eqs. (17) and (18) into Eqs. (6) and (7) gives the leading-order homogeneous convective wave equation for $\phi_{(s)}$:

$$\frac{\mathrm{D}_0}{\mathrm{D}t}\frac{1}{c_0^2}\frac{\mathrm{D}_0}{\mathrm{D}t}\phi_{(s)}^{(0)} - \frac{1}{\rho_0}\nabla\cdot(\rho_0\nabla)\phi_{(s)}^{(0)} = 0 \tag{19}$$

with the boundary condition of flow impermeability

$$\nabla\phi_{(s)}^{(0)}\cdot\boldsymbol{n} = -\boldsymbol{u}_{(i)}\cdot\boldsymbol{n} \tag{20}$$

imposed along the blade surface with normal $\boldsymbol{n}$. Higher-order terms of expansions (17) and (18) can be obtained by substituting $\phi_{(s)}^{(0)}$ into the right-hand side of Eq. (6) to calculate $\boldsymbol{u}_{(s)}^{(R)(1)}$. The solution to $\mathcal{O}(1/B)$ is then obtained by solving the nonhomogeneous equation (7), with the boundary condition

$$\left[\boldsymbol{u}_{(s)}^{(R)(1)} + \nabla\phi_{(s)}^{(1)}\right]\cdot\boldsymbol{n} = 0 \tag{21}$$

The numerical analysis of this paper is limited to determining leading-order term $\phi_{(s)}^{(0)}$ of the expansion (17). For simplicity we drop the superscript 0. The boundary-value interaction problem is thus formulated in terms of the homogeneous equation (19), with the blade boundary condition (20), the Kutta condition at the blade trailing edges, continuity of the unsteady pressure and normal velocity along the blade wakes, and upstream and downstream nonreflecting boundary conditions.

It is convenient to nondimensionalize all of the characteristic quantities, as follows. All lengths will be normalized by the projection of the blade semichord on the machine axis $c/2$; time t, by $c/2U_0$; the mean flow velocity components, by U_0; the velocity of the incident disturbance $\boldsymbol{u}_{(i)}$, by $\max|\boldsymbol{B}_m(x_0, r)|$; the potential response $\phi_{(s)}$ at each blade strip $r = r_s$, by $|B_m^{(n)}(0, r)|c/2$. To compare the results of the present analysis with two-dimensional strip theory, we normalize the unsteady pressure p', by $\bar{\rho}_0 U_x|B_m^{(n)}(0, r)|$, where $\bar{\rho}_0$ is the stagnation mean flow density and $|B_m^{(n)}(0, r)|$ is the upwash component of the incident velocity perturbation at the blade strip midchord position.

We also introduce the reduced frequency associated with the blade chord $k_{(s)} = \omega c/2U_0$ and the Mach numbers of the axial and swirl mean velocity components $M_x = U_x/\bar{c}_0$ ($\bar{M}_x = U_0/\bar{c}_0$), $M_\Gamma = \Gamma/r\bar{c}_0$ ($\bar{M}_\Gamma = \Gamma/r_m\bar{c}_0$), and $M_\Omega = \Omega r/\bar{c}_0$ ($\bar{M}_\Omega = \Omega r_m/\bar{c}_0$), where $\bar{c}_0$ is the stagnation mean flow speed of sound and r_m is the mean radius of the annulus, $r_m = (r_h + r_t)/2$, and r_h and r_t are the hub and tip radii of the annular duct. Finally, the number of blades in the row N_b is specified.

Numerical formulation in the frequency domain leads to the boundary-value problem for an elliptic three-dimensional partial differential equation with nonconstant, complex coefficients. The blades are assumed rigid, unloaded, and evenly spaced in the cascade situated in an infinite uniform annular duct. The assumption of evenly spaced cascade blades leads to the quasi-periodicity condition between the blades

$$\hat{\phi}_{(s)}(x, r, \theta + 2\pi/N_b) = \hat{\phi}_{(s)}(x, r, \theta)e^{i\sigma} \tag{22}$$

where $\sigma = 2\pi m/N_b$ is the interblade phase angle. Along the surfaces of the blade wakes with normal vector $\boldsymbol{n}$, pressure and normal velocity continuity is expressed by

$$\hat{p}'_{(s)}(x, r, \theta + 2\pi/N_b) = \hat{p}'_{(s)}(x, r, \theta)e^{i\sigma} \tag{23}$$

$$\left[\nabla\hat{\phi}_{(s)}\cdot\boldsymbol{n}\right](x, r, \theta + 2\pi/N_b) = \left[\nabla\hat{\phi}_{(s)}\cdot\boldsymbol{n}\right](x, r, \theta)e^{i\sigma} \tag{24}$$

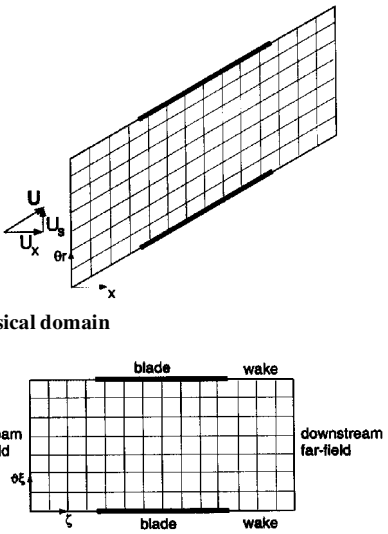

Fig. 1 Two-dimensional cut of the blade passage.

The solution is obtained for a single blade passage. The physical domain is curved as it extends downstream to remain aligned with the swirling streamlines of the mean flow. Therefore, the numerical solution of the boundary-value problem is obtained in the transformed coordinate system $[\zeta = x, \xi = r, \vartheta = \theta - (\Omega + \Gamma/r^2)x/U_x]$ (Fig. 1). The computational domain extends in the axial direction for $-T_x \le \zeta \le T_x$, in the radial direction for $r_h \le \xi \le r_t$, and in the circumferential direction for $0 \le \vartheta \le 2\pi/N_b$.

Inflow/Outflow Conditions

Upstream and downstream from the blade row, the far-field behavior of the scattered unsteady disturbances is governed by the eigenmode analysis of the governing equations.[18] The inflow/outflow conditions assume modal representation of the outgoing unsteady pressure waves and satisfy causality by setting to zero all of the modes entering the computational domain. This generalizes the method used by Fang and Atassi[13] and Atassi et al.[19] Such a filter provides a nonreflective solution throughout the physical space of the annular blade-row passage. Thus the nearly sonic solution can be approximated in terms of a truncated expansion of the nearly sonic eigenmodes $\Phi_{\nu_l,n}(r)$,

$$\hat{\phi}_{(s)}(x, r, \theta) = \sum_{l=-L}^{L}\sum_{n=1}^{N}\left(C_{\nu_l,n}^{(u,d)}\Phi_{\nu_l,n}(r)\exp\left\{i\left[\nu_l\theta + k_{\nu_l,n}^{(u,d)}x\right]\right\}\right) \tag{25}$$

where n and ν_l are the radial and circumferential modal numbers, respectively. Note that ν_l is determined from the cascade quasi-periodicity condition $\nu_l = m + lN_b$. The axial wave numbers $k_{\nu_l,n}^{(u)}$ and $k_{\nu_l,n}^{(d)}$ represent two families of eigenvalues obtained from the eigenmode analysis. In the frame of reference moving with the mean flow, these two families correspond to upstream and downstream propagating pressure–dominated scattered modes, respectively. The unknown constants $C_{\nu_l,n}^{(u,d)}$ will be defined numerically by matching the asymptotic far-field expansion with the solution of the boundary-value problem. We also introduce the normalized pressure mode

$$\mathcal{P}_{\nu_l,n}(r) = -\frac{i\rho_0}{M_x\bar{\rho}_0}\Lambda_{\nu_l,n}\Phi_{\nu_l,n}(r) \tag{26}$$

where $\Lambda_{\nu_l,n}$ is the normalized eigenvalue of the convected operator $\mathrm{D}_0/\mathrm{D}t$

$$\Lambda_{\nu_l,n} = \left[-k_{(s)}\bar{M}_x + k_{\nu_l,n}^{(u,d)}M_x + (\nu_l/r)(M_\Omega + M_\Gamma)\right]\Big|\ M_x \tag{27}$$

Because the eigenmode analysis uses a pseudospectral method,[18] spurious and nonphysical eigensolutions must be filtered out. In addition, causality imposes the condition that only outgoing propagating and evanescent pressure waves satisfying causality must be selected.

The inflow/outflow conditions are implemented in the form of impedence-type relations between the unsteady pressure and its convective derivative. This formulation is consistent with the condition of pressure continuity across the wakes of the blades. The conditions are applied at the upstream and downstream planes $x = x_{u,d}$ of the computational domain boundaries. They incorporate the expansion of the solution for the unsteady pressure in terms of the eigenmodes (26). The Fourier component of the pressure $\hat{p}'_{(s)}$ corresponding to $\hat{\phi}_{(s)}$ in Eq. (25) can be represented in the form of the vector product

$$\hat{p}'_{(s)}(x, r, \theta) = \boldsymbol{P}(x, r, \theta) \cdot \boldsymbol{C} \tag{28}$$

where

$$\boldsymbol{P}(x, r, \theta) = \begin{bmatrix} \mathcal{P}_{\nu_{-L},1}(r)\exp\left\{i\left[\nu_{-L}\theta + k^{(u,d)}_{\nu_{-L},1}\right]x\right\} \\ \mathcal{P}_{\nu_{-L},2}(r)\exp\left\{i\left[\nu_{-L}\theta + k^{(u,d)}_{\nu_{-L},2}\right]x\right\} \\ \vdots \\ \mathcal{P}_{\nu_{-L},N}(r)\exp\left\{i\left[\nu_{-L}\theta + k^{(u,d)}_{\nu_{-L},N}x\right]\right\} \\ \vdots \\ \mathcal{P}_{\nu_{L},N}(r)\exp\left\{i\left[\nu_{L}\theta + k^{(u,d)}_{\nu_{L},N}x\right]\right\} \end{bmatrix} \tag{29}$$

and $\boldsymbol{C} = \{C^{(u,d)}_{\nu_l,n}\}$ is the vector of unknown modal amplitudes.

To construct the matrix formulation of the inflow/outflow conditions, vector (29) is written for each of the $(2L + 1) \times N$ grid points (θ_i, r_j), $i = 1, \ldots, 2L + 1$, $j = 1, \ldots, N$ in the $x = x_{u,d}$ planes. The resulting vector of grid solutions $P(x) = \{\hat{p}'_{(s)}(x, r_j, \theta_i)\}$ is written in the form of the matrix-vector product

$$P(x) = \tilde{\boldsymbol{P}}(x) \cdot \boldsymbol{C} \tag{30}$$

with the rows of matrix $\tilde{\boldsymbol{P}}(x)$ filled with the transposed vectors $\boldsymbol{P}^T(x, r_j, \theta_i)$ for all chosen grid points

$$\tilde{\boldsymbol{P}}(x) = \left[\boldsymbol{P}^T(x, r_1, \theta_1) \cdots \boldsymbol{P}^T(x, r_N, \theta_1) \cdots \boldsymbol{P}^T(x, r_N, \theta_{2L+1})\right]^T \tag{31}$$

In the numerical ordering of the global matrix for the boundary-value problem, the points $(x_{u,d}, r_1, \theta_1)$ are placed along the diagonal of the matrix.

We now derive similar expressions for the Fourier component of the convected derivative of the unsteady pressure at the inflow/outflow boundaries. Thus, for each grid point at the planes $x = x_{u,d}$

$$\frac{\hat{\mathrm{D}}_0}{\mathrm{D}t} p'_{(s)}(x, r, \theta) = \boldsymbol{D}_p(x, r, \theta) \cdot \boldsymbol{C} \tag{32}$$

where

$$\boldsymbol{D}_p(x, r, \theta) = \begin{bmatrix} i\Lambda_{\nu_{-L},1}\mathcal{P}_{\nu_{-L},1}(r)\exp\left\{i\left[\nu_{-L}\theta + k^{(u,d)}_{\nu_{-L},1}x\right]\right\} \\ i\Lambda_{\nu_{-L},2}\mathcal{P}_{\nu_{-L},2}(r)\exp\left\{i\left[\nu_{-L}\theta + k^{(u,d)}_{\nu_{-L},2}x\right]\right\} \\ \vdots \\ i\Lambda_{\nu_{-L},N}\mathcal{P}_{\nu_{-L},N}(r)\exp\left\{i\left[\nu_{-L}\theta + k^{(u,d)}_{\nu_{-L},N}x\right]\right\} \\ \vdots \\ i\Lambda_{\nu_{L},N}\mathcal{P}_{\nu_{L},N}(r)\exp\left\{i\left[\nu_{L}\theta + k^{(u,d)}_{\nu_{L},N}x\right]\right\} \end{bmatrix} \tag{33}$$

The resulting grid vector $D_p(x) = \{\hat{\mathrm{D}}_0 p'_{(s)}(x, r_j, \theta_i)/\mathrm{D}t\}$ is represented as follows:

$$D_p(x) = \tilde{\boldsymbol{D}}_p(x) \cdot \boldsymbol{C} \tag{34}$$

where

$$\tilde{\boldsymbol{D}}_p(x) = \left[\boldsymbol{D}^T_p(x, r_1, \theta_1) \cdots \boldsymbol{D}^T_p(x, r_N, \theta_1) \cdots \boldsymbol{D}^T_p(x, r_N, \theta_{2L+1})\right]^T \tag{35}$$

Substituting the vector of modal coefficients from Eq. (30) into Eq. (34), we derive the following impedence-type relation:

$$D_p = \tilde{\boldsymbol{D}}_p \cdot \tilde{\boldsymbol{P}}^{-1} \cdot P \tag{36}$$

This expression can be further simplified because the terms $\exp[ik^{(u,d)}_{\nu_l,n}x]$ drop out in the preceding matrix product. As a result, numerical implementation of the inflow/outflow conditions for each grid point reduces to the form

$$\frac{\partial \hat{p}'_{(s)}}{\partial \zeta} - ik_{(s)}\frac{\bar{M}_x}{M_x}\hat{p}'_{(s)} - \boldsymbol{R}^T \cdot [\tilde{\boldsymbol{D}}^* \cdot (\tilde{\boldsymbol{P}}^*)^{-1} \cdot P] = 0 \tag{37}$$

where $\boldsymbol{R} = (1, 0, \ldots, 0)$ is a vector of $(2L + 1) \times N$ elements and $\tilde{\boldsymbol{P}}^* = [\mathcal{P}_{\nu_l,n}(r_n)\exp(i\nu_l\theta_i)]$ and $\tilde{\boldsymbol{D}}^* = [i\Lambda_{\nu_l,n}\mathcal{P}_{\nu_l,n}(r_n)\exp(i\nu_l\theta_i)]$ are matrices. In expansion (25) N is limited by the number of grid points in the radial direction, and $(2L + 1)$ by that in the circumferential direction. In practice, one may choose the number of terms in the truncated series less than the number of grid points. In this case the best accuracy is obtained if we neglect the terms corresponding to rapidly decaying modes with high $Im[k^{(u,d)}_{\nu_l,n}]$.

The inflow and outflow computational boundaries are located only a short distance away from the blades (of the order of blade chord). Hence, the evanescent modes will contribute to the unsteady pressure levels at these boundaries. The close location of the inflow/outflow boundaries to the blades is primarily imposed by the computational requirements. It would be advantageous to increase the number of grid points by using efficient iterative solvers such as a generalized minimal residual algorithm (GMRES). However, such solvers so far failed to provide a reliable convergent solution to the complex algebraic system of equations resulting from the numerical discretization of the unsteady interaction problem. This is in part related to the dense fill-in of rows of the boundary-value problem matrix at the inflow/outflow boundaries, in contrast to a typically sparse fill-in of the matrix rows elsewhere. This appears to deteriorate the overall matrix condition number and results in convergence failures for the iterative solvers. To limit the number of terms in the expansion (25) and thus improve the matrix, we limit expansion (25) to all propagating modes and to those evanescent modes satisfying the criterion

$$\left|\exp\left[ik^{(u,d)}_{\nu_l,n}(x_{u,d} \pm 1)\right]\right| \geq 0.01 \tag{38}$$

where + is taken at the upstream boundary and − at the downstream boundary.

Direct solvers have significant computer memory requirements for matrix storage and inversion. For higher reduced frequencies these requirements increase because more grid points are needed to resolve and propagate the pressure modes to the far field. Moreover, the problem of wave resolution is more severe for modes propagating in a swirling mean flow. As illustrated in the numerical examples shown next, the Doppler effect spreads the axial wave numbers $k^{(u,d)}_{\nu_l,n}$ of acoustic and evanescent modes over a much wider range compared to the uniform flow. As a result of this wave dispersion, one needs to resolve the waveforms over a wider range of modal wavelengths, which requires smaller mesh size in the numerical discretization.

Comparison with Two-Dimensional Model

In the classical two-dimensional cascade theory of the unrolled cascade (e.g., Ref. 3), the stationary velocity perturbation is represented in the orthogonal coordinates $\boldsymbol{X} = (X_1, X_2, X_3)$, with the X_1 axis aligned with the mean flow and X_3 axis in the span direction

$$\boldsymbol{u}^{(2D)}_{(i)} = \boldsymbol{B}^{(2D)}(X_3)e^{imX_2/r\cos\nu} \tag{39}$$

where $\nu = \tan^{-1} U_s/U_x$ is the flow swirl angle. $\boldsymbol{B}^{(2D)}(X_3)$ is the frozen stationary gust velocity amplitude vector, which can be written in the form

$$\boldsymbol{B}^{(2D)}(X_3) = (A_{m,q}\hat{\boldsymbol{I}}_1 + B_{m,q}\hat{\boldsymbol{I}}_2)\cos(\pi q X_3/b) + (A'_{m,q}\hat{\boldsymbol{I}}_1 + C_{m,q}\hat{\boldsymbol{I}}_3)\sin(\pi q X_3/b) \quad (40)$$

where $\hat{\boldsymbol{I}}_1$, $\hat{\boldsymbol{I}}_2$, and $\hat{\boldsymbol{I}}_3$ are unit vectors in the X_1, X_2, and X_3 directions; $A_{m,q}$, $A'_{m,q}$, $B_{m,q}$, and $C_{m,q}$ are constant complex amplitudes of the gust harmonic coupled by the divergence-free condition

$$\frac{im}{\pi r\cos\nu}B_{m,q} + \frac{q}{b}C_{m,q} = 0 \quad (41)$$

and $q = 0, 1, 2, \ldots$. The term with $A'_{m,q}$ is commonly omitted in two-dimensional theories that, because of the radial symmetry, do not contribute to the cascade unsteady response. Note, however, that it does contribute in three-dimensional theory. Usually the first term of the imposed disturbance velocity (40) models velocity defects in the wakes of an upstream cascade, whereas the other two terms may represent unsteady secondary flows produced in the turbomachinery annulus.

For the two-dimensional model the formulation of the boundary-value gust-cascade interaction problem is equivalent for both cases of rotor/stator and stator/rotor interactions and may be reduced to an integral equation for the unsteady pressure jump across the blade surface. The early treatments solved numerically the integral equation in a frame of reference fixed with the downstream cascade blades $\boldsymbol{Y} = (Y_1, Y_2, Y_3)$ with an upwash velocity component of the sinusoidal gust

$$\boldsymbol{u}^{(2D)}_{(i)} = \boldsymbol{a}e^{i(\boldsymbol{k}\cdot\boldsymbol{Y} - \omega t)} \quad (42)$$

where $\boldsymbol{a} = \{a_1, a_2, a_3\}$ and $\boldsymbol{k} = \{k_1, k_2, k_3\}$ represent, respectively, the gust amplitude and wave vectors in the $\boldsymbol{Y}$ coordinates. Only the *upwash* gust component a_2 will contribute to the unsteady response of the blades.

Interstage Interaction

We now apply the boundary-value analysis to model the unsteady interrow interaction. We consider only vortical incident disturbances. The case of incident acoustic disturbances can be treated in a similar way.

We examine separately two different cases of this turbomachinery interaction corresponding to stator/rotor and rotor/stator interactions as shown in Figs. 2 and 3. The schematic views are shown from above of the stator and rotor blade rows at a radius r of the turbomachinery annulus. The rotor is rotating with an angular velocity Ω_R so that at radius r the circumferential velocity $U_c = \Omega_R r$.

Stator/Rotor Interaction

Upstream of the rotor stage in Fig. 2, a specified stationary perturbation $\boldsymbol{u}_{(i)}$ is imposed on a swirling mean motion. In the

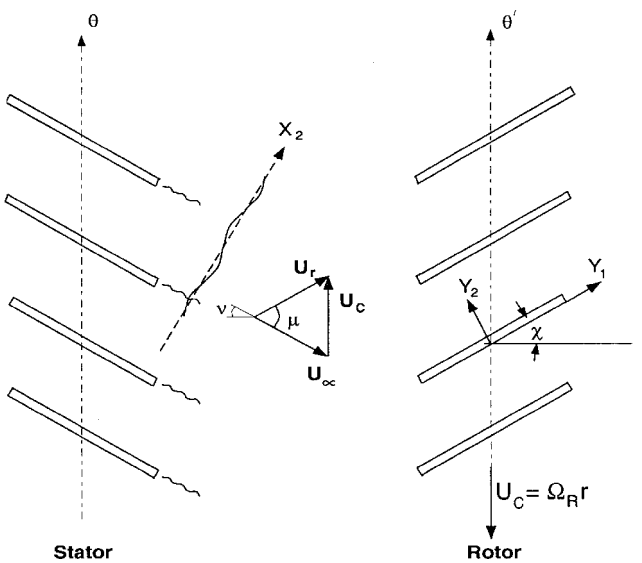

Fig. 2 Stator/rotor vortical interaction.

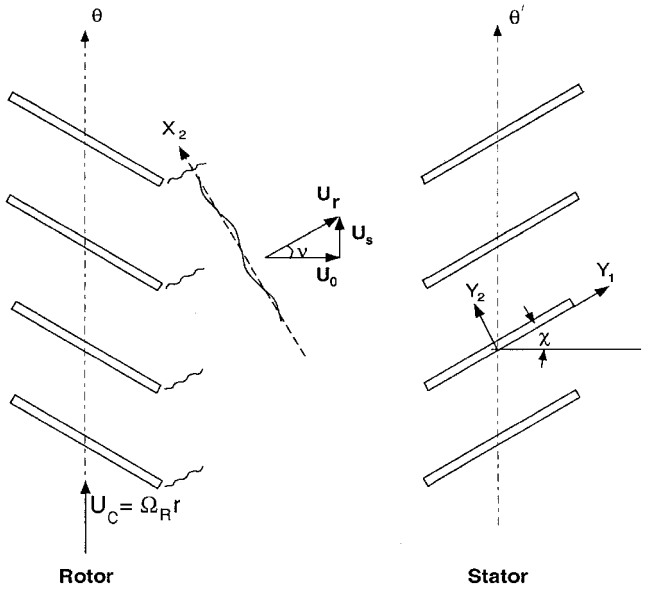

Fig. 3 Rotor/stator vortical interaction.

stator frame of reference (x, r, θ), the total mean flow velocity is $\boldsymbol{U}_\infty = U_x\hat{e}_x + U_s\hat{e}_\theta$, and the stationary perturbation models the wake velocity defects induced by the stator blades.

In the rotor frame of reference (x, r, θ'), the total mean velocity $\boldsymbol{U}_r = U_x\hat{e}_x + (U_s + \Omega_R r)\hat{e}_{\theta'}$ is at angle μ with $\boldsymbol{U}_\infty$. For an unloaded cascade the blades are set at a stagger angle χ to provide zero angles of attack for the blades ($\chi = \mu - \nu$). In this frame of reference, the gust perturbation appears unsteady in view of the relation $\theta = \theta' - \Omega_R t$.

For the two-dimensional model it is convenient to express the incident disturbances in terms of a coordinate system in the rotor frame of reference

$$X_2 = Y_1\sin\mu + Y_2\cos\mu - \Omega_R r t\cos\nu \quad (43)$$

so that for the rotor stage, the gust velocity (39) transforms to

$$\boldsymbol{u}^{(2D)}_{(i)}(Y_1, Y_2, Y_3) = \boldsymbol{a}\exp\left(im\Omega_R\left(\frac{Y_1}{U_r} + \frac{Y_2\cot\mu}{U_r} - t\right)\right) \quad (44)$$

The contributing upwash component of the local gust velocity is easily deduced:

$$a_2 = -A_{m,q}\sin\mu + B_{m,q}\cos\mu \quad (45)$$

with the wave vector components $k_1 = m\Omega_R/U_r$, $k_2 = k_1\cot\mu$, $k_3 = \pi q/b$ (U_r is the magnitude of $\boldsymbol{U}_r$).

In the three-dimensional problem the stationary gust (12) in the rotor frame of reference (x, r, θ') becomes

$$\boldsymbol{u}_{(i)}(x, r, \theta) = \boldsymbol{B}_m(x, r)\exp[im(\theta' - \Omega_R t)] \quad (46)$$

The boundary-value interaction problem is then solved numerically in the moving rotor frame of reference by transforming the gust solution to the computational domain with $\vartheta = \theta' - (U_s + \Omega_R r)x/rU_x - \Omega_R t$.

Rotor/Stator Interaction

In the case of the rotor/stator interaction (Fig. 3), the disturbance will appear stationary in the rotor frame of reference where we assume it to be of the form $\boldsymbol{u}_{(i)} \sim \exp(im\theta)$. In the stationary stator coordinates the wake-induced perturbation is viewed as unsteady because $\theta' = \theta + \Omega_R t$. The unsteady disturbance evolves in the swirling mean motion and interacts with the stator row of blades aligned with the swirling streamlines of the mean flow ($\chi = \nu$).

As before, expression (39) describes the imposed gust velocity perturbation in the two-dimensional cascade model [$\boldsymbol{X} = (X_1, X_2, X_3)$ are now rotor coordinates aligned with the downstream

flow streamlines]. Transformation to the stationary coordinates $\boldsymbol{Y}$ and (x, r, θ') of the stator blades and the duct gives

$$X_2 = Y_2 - \Omega_R r \tau \cos\nu = r\theta' \cos\nu - x \sin\nu - \Omega_R r \tau \cos\nu \quad (47)$$

where the retarded time is introduced $\tau = t - x/U_x$. Because $\mu = 0$ in this case, the upwash amplitude of the sinusoidal gust (42) is $a_2 = B_{m,q}$, and the wave vector components are $k_1 = m\Omega_R/U_r$, $k_2 = m/r\cos\nu - k_1 \tan\nu$, $k_3 = \pi q/b$.

The initial-value problem for the three-dimensional gust evolution is solved in the duct coordinates in which the disturbance is of the form (46). The boundary-value problem for the gust response is formulated in the transformed coordinates aligned with the swirling streamlines of the mean flow with $\vartheta = \theta' - xU_s/rU_x$.

Results and Discussion

The results obtained from our three-dimensional numerical code GENGUS solving the generalized gust problem in a swirling mean flow are compared with two-dimensional strip theory calculations. The three-dimensional code solves the boundary-value problem in the frequency domain and employs a second-order accurate finite difference approximation for the governing equation (19) and the corresponding boundary conditions. In particular, a 15-point central differencing is applied to discretize Eq. (19), and a 7-point one-sided differencing is used to discretize the blade boundary condition (20).

A linear system of equations resulting from the numerical discretizataion of the boundary-value problem is solved using a direct sparse matrix solver.[20] An IBM RISC 6000-590 computer system is used in all computations. Stringent computer memory requirements are satisfied by choosing the extent of the computational domain in the axial direction $2T_x = 5$ and the number of grid points in the (x, r, θ) directions $N_x \times N_r \times N_\theta = 100 \times 20 \times 15$. Because we are solving for the potential function, this defines the total number of complex unknowns in the problem equal to 30,000. Based on the results of Ref. 19, a minimum of 15 points per wavelength is required to properly resolve acoustic modes using a second-order discretization scheme and thus provide an adequate link between the near-field aerodynamic solution and the far-field unsteady flow conditions at the inlet and outlet boundaries of the computational domain. Hence, the number of grid points is selected to satisfy this criterion for all acoustic modes in the cases discussed next.

The results for the scattered field (unsteady blade response) are examined for the case of the rotor/stator vortical interaction illustrated in Fig. 3. For the numerical computations we consider an annular duct with hub and tip radii $r_h = 3$ and $r_t = 5$, respectively. The upstream rotor cascade has 20 blades; hence, $m = 20$ for the first harmonic of the wake-induced velocity perturbation (39), which we consider in the numerical example. The number of blades in the stator cascade is taken $N_b = 15$, which provides a midspan cascade spacing $\bar{s} = 2\pi r_m/N_b \simeq 1.7$ (normalized, as all other lengths, by the projection of blade semichord on the machine axis $c/2$).

The frequency of the stator unsteady response is determined by $\omega = m\Omega_R$. This defines the reduced frequency of the interaction problem $k_{(s)} = (m/r_m)\bar{M}_R/\bar{M}_x$, where $\bar{M}_R = \Omega_R r_m/\bar{c}_0$. For the calculations we take $\bar{M}_x = 0.644$ and the ratio $\bar{M}_R/\bar{M}_x = 0.6$; hence, $k_{(s)} = 3$.

For the mean swirl we examine two cases. The first case, with $\bar{M}_\Gamma = 0.212$ and $\bar{M}_\Omega = 0.033$, corresponds to the swirl distribution of a typical turbofan engine. The swirl for this fan design is close to that of a free vortex. For the second case we take a mean flow swirl with larger vorticity $\bar{M}_\Gamma = 0.1$ and $\bar{M}_\Omega = 0.2$. Figure 4 illustrates the radial variation of the mean flow parameters in both cases.

We carry out an eigenvalue analysis[18] to determine the eigenmodes to be included in the expansion (25) for the inflow/outflow boundary conditions. Figure 5 shows the eigenvalues for different circumferential modal numbers $\nu_l = m + lN_b$ and radial modal numbers $n = 1, \ldots, 12$, with $l = -7, \ldots, 7$. The modes from the first quadrant of the complex $k_{\nu_l,n}$ plane propagate or decay downstream, whereas those from the third quadrant, they appear upstream. In both cases of the mean swirl, there are four cut-on modes upstream and two downstream. Most of the propagating modes correspond to $\nu_l < 0$ and thus spin opposite to the mean swirl direction. The differences between the two cases are mostly attributed to the effects of refraction and Doppler shift on the acoustic resonance conditions.

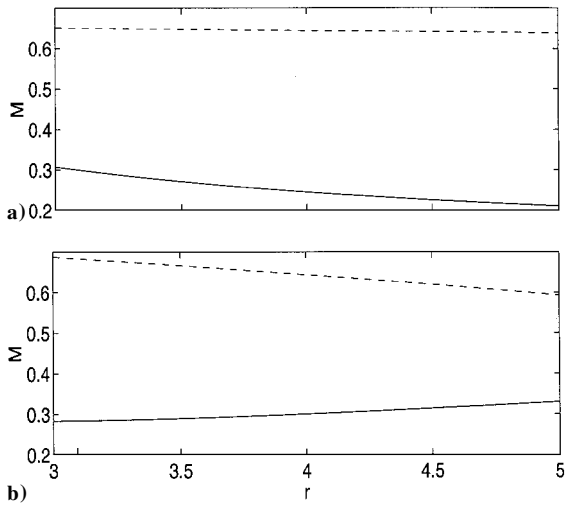

Fig. 4 Mean velocity Mach numbers for the axial (– – –) and swirling (——) components; $\bar{M}_x = 0.644$: a) $\bar{M}_\Omega = 0.033$, $\bar{M}_\Gamma = 0.212$; and b) $\bar{M}_\Omega = 0.2$, $\bar{M}_\Gamma = 0.1$.

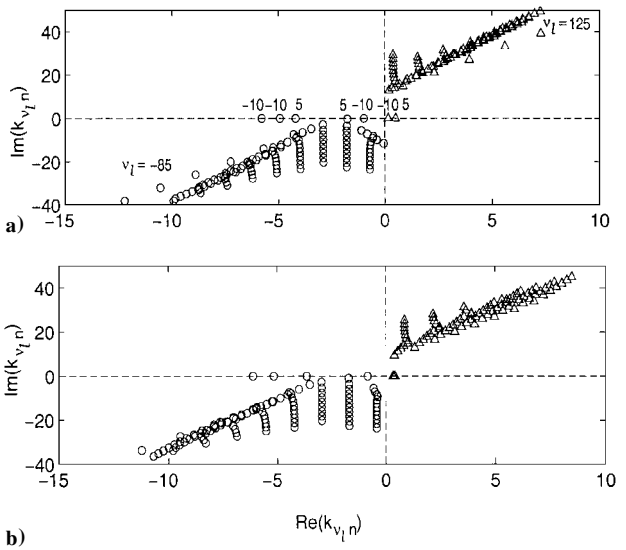

Fig. 5 Eigenvalues for upstream (○) and downstream (△) pressure modes; $\bar{M}_x = 0.644$, $k_{(s)} = 3$, $m = 20$: a) $\bar{M}_\Omega = 0.033$, $\bar{M}_\Gamma = 0.212$; and b) $\bar{M}_\Omega = 0.2$, $\bar{M}_\Gamma = 0.1$.

Many upstream-propagating evanescent modes have small rates of decay, and thus may contribute to the level of unsteady pressure at the upstream boundary of the computational domain. Based on the criterion (38), seven evanescent modes have been included in the expansion (25) at the upstream computational boundary.

To validate our leading-order analysis of Eqs. (6) and (7), we show, in Table 1, the ratio $|\Lambda_{\nu_l,n}/\Omega|$ for propagating modes in the two cases discussed. This ratio is smaller (as expected) for the second case where vortical swirl component is dominant. Still, in both cases this ratio is high enough to validate the approach.

The unsteady aerodynamic response of the stator blade is characterized in terms of the normalized unsteady pressure jump across the blades $C_p^s(x) = \Delta p'(x, r)$, specified at the blade strip $s = (r - r_h)/(r_t - r_h)$. In the two-dimensional analysis[5] the parameters of the mean flow and cascade geometry are recalculated for each blade strip. We first compare the two- and three-dimensional calculations to examine the effects of geometry and acoustic eigenmodes on the unsteady blade pressure. To this end, we remove the effects of the upwash evolution caused by the swirl and only consider a frozen convected gust upwash with amplitude $B_m^{(n)} = a_2 = 1$, for $q = 0$ ($k_3 = 0$). The results in Figs. 6 and 7 are presented for $C_p^s(x)$ along the midspan blade strip $s = 0.5$. In both cases of the mean flow, the results for the magnitude of the unsteady response are in good agreement for the two models. On the other hand, significant phase differences are evident, especially near the leading edge

Table 1 Ratio $|\Lambda_{\nu_l,n}/\Omega|$ for propagating acoustic modes

$(\nu_l, n)^{(u,d)}$	$k_{\nu_l,n}^{(u,d)}$	$\lvert\Lambda_{\nu_l,n}/\Omega\rvert$
Case 1 ($\bar{M}_\Gamma = 0.212$, $\bar{M}_\Omega = 0.033$)		
$(5, 1)^{(u)}$	−4.2	516
$(-10, 1)^{(u)}$	−5.8	787
$(-10, 2)^{(u)}$	−4.9	720
$(5, 1)^{(d)}$	0.5	145
$(-10, 1)^{(d)}$	0.17	319
$(-10, 2)^{(d)}$	−0.98	409
Case 2 ($\bar{M}_\Gamma = 0.1$, $\bar{M}_\Omega = 0.2$)		
$(5, 1)^{(u)}$	−3.8	81
$(-10, 1)^{(u)}$	−6.1	137
$(-10, 2)^{(u)}$	−5.1	124
$(5, 1)^{(d)}$	0.43	24
$(-10, 1)^{(d)}$	0.36	51
$(-10, 2)^{(d)}$	−0.85	67

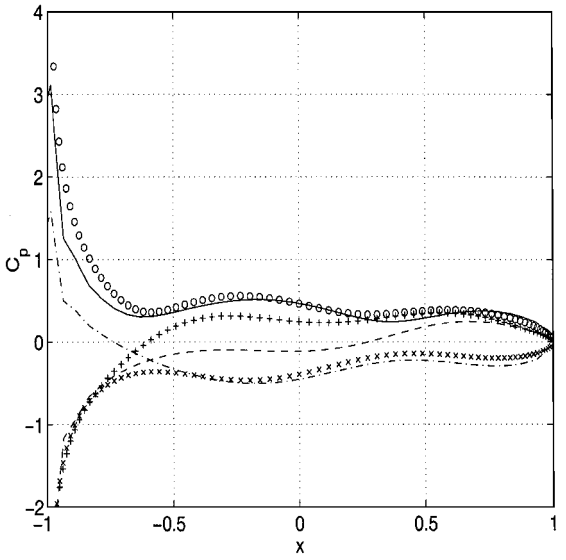

Fig. 6 Aerodynamic gust response at the blade strip $s = 0.5$ for $\bar{M}_x = 0.644$, $\bar{M}_\Omega = 0.033$, $\bar{M}_\Gamma = 0.212$, $k_{(s)} = 3$, $B_m^{(n)} = 1$, $m = 20$, $q = 0$: numerical analysis: $|C_p|$ (——), $Re(C_p)$ (– – –), $Im(C_p)$ (– ·–); strip theory: $|C_p|$ (○), $Re(C_p)$ (+), $Im(C_p)$ (×).

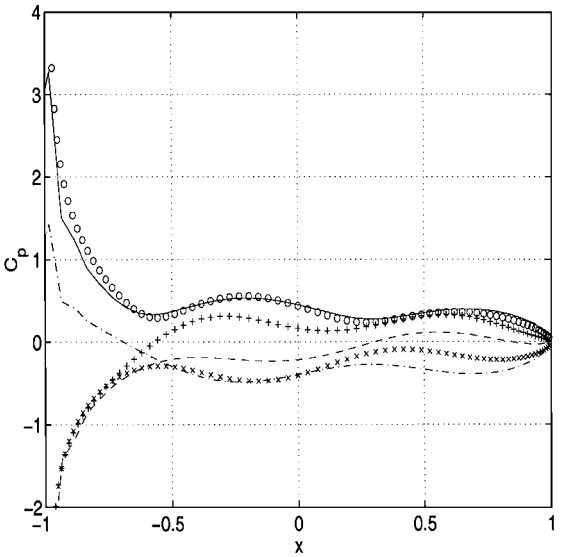

Fig. 7 Aerodynamic gust response C_p at the blade strip $s = 0.5$ for $\bar{M}_x = 0.644$, $\bar{M}_\Omega = 0.2$, $\bar{M}_\Gamma = 0.1$, $k_{(s)} = 3$, $B_m^{(n)} = 1$, $m = 20$, $q = 0$; numerical analysis: $|C_p|$ (——), $Re(C_p)$ (– – –), $Im(C_p)$ (– ·–); strip theory: $|C_p|$ (○), $Re(C_p)$ (+), $Im(C_p)$ (×).

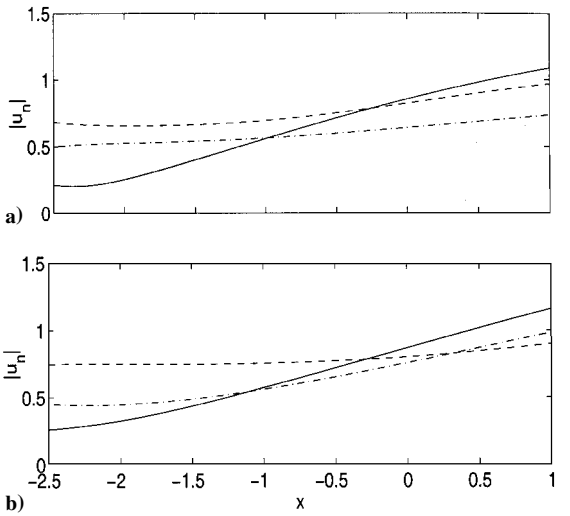

Fig. 8 Downstream evolution of the gust upwash $B_m^{(n)}(x, r)$ along the strips $s = 0.75$ (– ·–), $s = 0.5$ (——), $s = 0.25$ (– – –); $\bar{M}_x = 0.644$, $k_{(s)} = 3$, $A_{\theta mq} = 1$, $m = 20$, $q = 1$: a) $\bar{M}_\Omega = 0.033$, $\bar{M}_\Gamma = 0.212$; and b) $\bar{M}_\Omega = 0.2$, $\bar{M}_\Gamma = 0.1$.

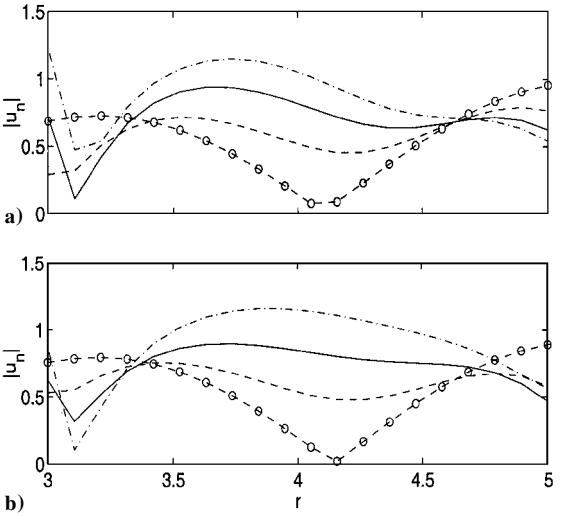

Fig. 9 Modification of the radial profile of the gust upwash $B_m^{(n)}(x, r)$ from the initial position $x_0 = -2.5$ (○) to the blade leading edge $x = -1$ (– – –), midchord $x = 0$ (——), trailing edge $x = 1$ (– ·–) for $\bar{M}_x = 0.644$, $k_{(s)} = 3$, $A_{\theta mq} = 1$, $m = 20$, $q = 1$: a) $\bar{M}_\Omega = 0.033$, $\bar{M}_\Gamma = 0.212$; and b) $\bar{M}_\Omega = 0.2$, $\bar{M}_\Gamma = 0.1$.

where $Im(C_p)$ obtained from the numerical analysis diverges from the strip theory predictions. We presume that these discrepancies result from high sensitivity of the phase to the effects of geometry, mean flow, and numerical discretization in presence of the numerous cut-on modes existing in a swirling flow.

We now examine the effect of the gust evolution on the aerodynamic response of the stator cascade. Figure 8 shows the downstream evolution (along the mean flow streamline) of the gust velocity upwash for the vortical disturbance imposed $\frac{3}{4}$ of the chord upstream from the blade leading edge, with the initial perturbation $A_{\theta mq} = 1$, $A_{rmq} = A_{xmq} = B_{xmq} = 0$, $m = 20$, and $q = 1$. In both cases of the mean swirl, the effect of the gust evolution is most pronounced at the midspan section of the chord $-1 \le x \le 1$. Figure 9 shows significant changes of the radial profile of the gust upwash along the blade chord. The increase of the upwash near the midspan region suggests that the effect of the gust radial profile change on the cascade response will be more significant at the blade midspan.

In Figs. 10 and 11 we present the three-dimensional calculations for the blade unsteady pressure. To determine the effects of the gust upwash evolution caused by the mean swirl, we compare the unsteady blade pressure obtained in our numerical calculations for an evolving gust (solid line) with two cases of a strip theory calculations for purely convected gusts. For the first case (marked by x) the frozen

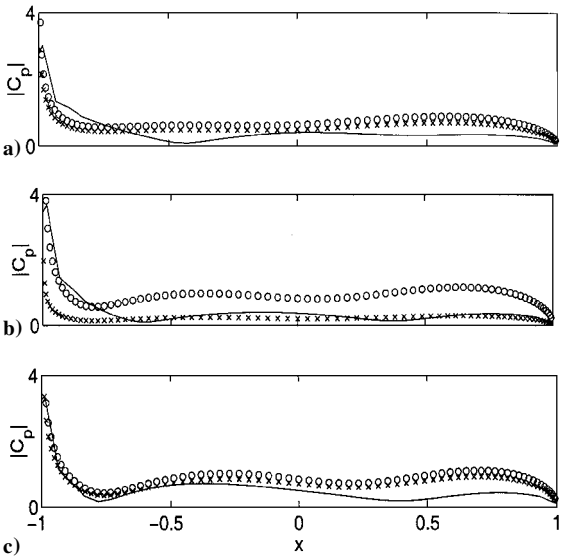

Fig. 10 Aerodynamic gust response $|C_p|$ at the blade strips a) $s = 0.75$, b) $s = 0.5$, c) $s = 0.25$ for $\bar{M}_x = 0.644$, $\bar{M}_\Omega = 0.033$, $\bar{M}_\Gamma = 0.212$, $k_{(s)} = 3$, $A_{\theta mq} = 1$, $m = 20$, $q = 1$: numerical analysis (——), strip theory with $a_2 = B_m^{(n)}(0, r)$ (○), and strip theory with $a_2 = B_m^{(n)}(x_0, r)$ (×).

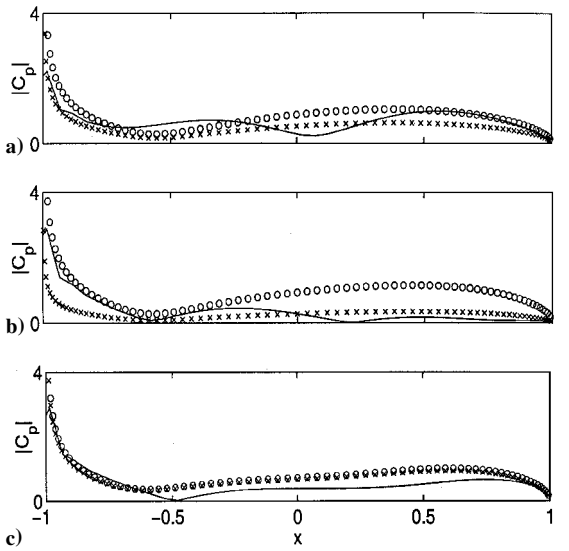

Fig. 11 Aerodynamic gust response $|C_p|$ at the blade strips a) $s = 0.75$, b) $s = 0.5$, c) $s = 0.25$ for $\bar{M}_x = 0.644$, $\bar{M}_\Omega = 0.2$, $\bar{M}_\Gamma = 0.1$, $k_{(s)} = 3$, $A_{\theta mq} = 1$, $m = 20, q = 1$: numerical analysis (——), strip theory with $a_2 = B_m^{(n)}(0, r)$ (○), and strip theory with $a_2 = B_m^{(n)}(x_0, r)$ (×).

gust amplitude is the same as the initial gust amplitude at x_0, and for the second (in circles) the frozen gust amplitude is the same as that of the evolving gust at midchord. The comparison is presented at three blade strips: $s = \frac{1}{4}, \frac{1}{2}$, and $\frac{3}{4}$. The two-dimensional results with the midchord gust input closely predict the full three-dimensional computations near the leading edge, but the comparison is worse further along the chord. This can be attributed mainly to the fact that the radial profile of the gust upwash undergoes a significant change from its initially harmonic distribution. In particular, the modification of the profile of the initial $q = 1$ perturbation along the chord (in Fig. 9) suggests that a better comparison could be achieved by considering the $q = 0$ harmonic in the strip theory analysis. This assumption is examined and confirmed in Fig. 12 by comparing the three-dimensional analysis (solid line) with two strip theory calculations for $q = 0$ (×) and $q = 1$ (○). Note that the unsteady pressure is larger for the $q = 1$ case. This results from a change from subcritical to supercritical regimes in the unsteady airfoil theory when $k_3 \sim k_1$ (Ref. 1).

These results suggest that the strip theory can be used to predict the effects of the mean swirl on the blade aerodynamic response by

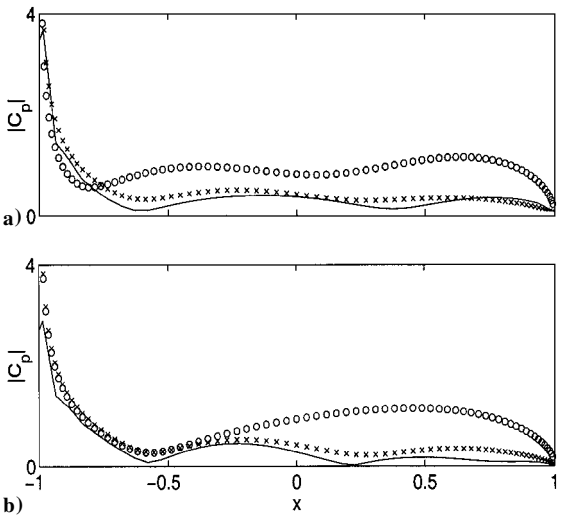

Fig. 12 Aerodynamic gust response $|C_p|$ at the blade strip $s = 0.5$ for $\bar{M}_x = 0.644$, $k_{(s)} = 3$, $A_{\theta mq} = 1$, $m = 20$, $q = 1$: numerical analysis (——), strip theory with $a_2 = B_m^{(n)}(0, r)$, $q = 1$ (○), and strip theory with $a_2 = B_m^{(n)}(0, r)$, $q = 0$ (×); a) $\bar{M}_\Omega = 0.033$, $\bar{M}_\Gamma = 0.212$; and b) $\bar{M}_\Omega = 0.2$, $\bar{M}_\Gamma = 0.1$.

incorporating the initial-value analysis of the gust upwash evolution and calculating the responses to each of its radial and axial Fourier components along the blade surface.

Conclusions

A model has been developed for the interaction of unsteady incident disturbances in a swirling mean motion with an annular cascade of unloaded blades. The incident disturbances are modeled using a combined eigenmode analysis with initial-value problem solutions as described in Part 1 of this paper. For simplicity, the mean flow swirl is represented as the sum of a free vortex and a rigid body rotation. The axial and radial distribution of the amplitude and phase of these disturbances change significantly as they propagate downstream. The boundary-value problem for the annular cascade has been formulated and solved numerically in an interblade passage domain. The computational domain extends $\frac{3}{4}$ of a blade chord length upstream and downstream of the leading and trailing edges, respectively. An impedence-type condition is derived for the inflow/outflow boundaries of the computational domain. This condition uses the nearly sonic pressure-dominated modes of the eigenmode expansion.

The scattered field is calculated in response to the blade upwash and accounts for the effects of the centrifugal and Coriolis forces induced by the mean swirl. Benchmark results for the unsteady blade pressure in the rotor-wake/stator interaction problem are presented for two mean swirl distributions. The average swirl angle is about 25 deg. The results are compared with strip theory for different spanwise locations and show strong dependence on the axial and radial evolution of the incident vortical disturbances.

Acknowledgments

The research was supported by Office of Naval Research Grant N00014-92-J-1165 and monitored by L. Patrick Purtell.

References

[1] Atassi, H. M., "Unsteady Aerodynamics of Vortical Flows: Early and Recent Developments," *Aerodynamics and Aeroacoustics*, edited by K.-Y. Fung, World Scientific, Singapore, 1994, pp. 121–172.

[2] Kaji, S., and Okazaki, T., "Propagation of Sound Waves Through a Blade Row. II. Analysis Based on the Acceleration Potential Method," *Journal of Sound and Vibration*, Vol. 11, No. 3, 1970, pp. 355–375.

[3] Goldstein, M. E., *Aeroacoustics*, McGraw–Hill, New York, 1976, p. 228.

[4] Smith, S. N., "Discrete Frequency Sound Generation in Axial Flows of Turbomachines," Aeronautical Research Council, R&M, No. 3709, Univ. Engineering Dept., Cambridge, England, U.K., March 1972.

[5] Ventres, C. S., "A Computer Program to Calculate Cascade 2D Kernel," NASA TM, Oct. 1980.

[6] Kaji, S., and Okazaki, T., "Generation of Sound by Rotor-Stator Interaction," *Journal of Sound and Vibration*, Vol. 13, No. 3, 1970, pp. 281–307.

[7]Hamad, G., and Atassi, H. M., "Sound Generated in a Cascade by 3D Disturbances Convected in a Subsonic Flow," AIAA Paper 81-2046, Oct. 1981.

[8]Goldstein, M. E., and Atassi, H. M., "A Complete Second-Order Theory for the Unsteady Flow About an Airfoil due to a Periodic Gust," *Journal of Fluid Mechanics*, Vol. 74, Pt. 4, 1976, pp. 741–765.

[9]Goldstein, M. E., "Unsteady Vortical and Entropic Distortions of Potential Flows Round Arbitrary Obstacles," *Journal of Fluid Mechanics*, Vol. 89, Pt. 3, 1978, pp. 433–468.

[10]Atassi, H. M., and Grzedzinski, J., "Unsteady Disturbances of Streaming Motions Around Bodies," *Journal of Fluid Mechanics*, Vol. 209, 1989, pp. 385–403.

[11]Scott, J. R., and Atassi, H. M., "A Finite-Difference Frequency Domain Numerical Scheme for the Solution of the Gust Response Problem," *Journal of Computational Physics*, Vol. 119, 1995, pp. 75–93.

[12]Hall, K. C., and Verdon, J. M., "Gust Response Analysis for Cascades Operating in Nonuniform Mean Flows," *AIAA Journal*, Vol. 29, No. 9, 1991, pp. 1463–1471.

[13]Fang, J., and Atassi, H. M., "Compressible Flows with Vortical Disturbances Around a Cascade of Loaded Airfoils," *Unsteady Aerodynamics, Aeroacoustics, and Aeroelasticity of Turbomachines and Propellers*, edited by H. M. Atassi, Springer-Verlag, New York, 1993, pp. 149–176.

[14]Namba, M., "Three-Dimensional Flows," *AGARD Manual an Aeroelasticity in Axial-Flow Turbomachines*, Vol. 1, *Unsteady Turbomachinery Aerodynamics*, edited by M. F. Platzer and F. O. Carta, AG-298, AGARD, 1987, pp. 75–104.

[15]Montgomery, M. D., and Verdon, J. M., "A Three-Dimensional Linearized Unsteady Euler Analysis for Turbomachinery Blade Rows," NASA CR-4770, March 1997.

[16]Golubev, V. V., and Atassi, H. M., "Unsteady Swirling Flows in Annular Cascades, Part 1: Evolution of Incident Disturbances," *AIAA Journal*, Vol. 38, No. 7, 2000, pp. 1142–1149.

[17]Golubev, V. V., and Atassi, H. M., "Sound Propagation in an Annular Duct with Mean Potential Swirling Flow," *Journal of Sound and Vibration*, Vol. 198, No. 5, 1996, pp. 601–616.

[18]Golubev, V. V., and Atassi, H. M., "Acoustic-Vorticity Waves in Swirling Flows," *Journal of Sound and Vibration*, Vol. 209, No. 2, 1998, pp. 203–222.

[19]Atassi, H. M., Fang, J., and Patrick, S., "Direct Calculation of Sound Radiated from Bodies in Nonuniform Flows," *Journal of Fluids Engineering*, Vol. 115, 1993, pp. 573–579.

[20]Eisenstat, S. C., Gursky, M. C., Schultz, M. H., and Sherman, A. H., "Yale Sparse Matrix Package II. The Nonsymmetric Codes," Dept. of Computer Science, Research Rept. 114, Yale Univ., New Haven, CT.

S. Glegg
Associate Editor